

# Carbon Nanotubes Embedded in Oriented Polymer Nanofibers by Electrospinning

Yael Dror,<sup>†</sup> Wael Salalha,<sup>‡</sup> Rafail L. Khalfin,<sup>†</sup> Yachin Cohen,<sup>\*,†</sup>  
Alexander L. Yarin,<sup>‡</sup> and Eyal Zussman<sup>‡</sup>

Departments of Mechanical Engineering and Chemical Engineering,  
Technion—Israel Institute of Technology, Haifa, Israel 32000

Received February 11, 2003. In Final Form: May 26, 2003

The electrospinning process was used successfully to fabricate nanofibers of poly(ethylene oxide) (PEO) in which multiwalled carbon nanotubes (MWCNT) are embedded. Initial dispersion of MWCNTs in water was achieved using amphiphiles, either as small molecules (sodium dodecyl sulfate, SDS) or as a high molecular weight, highly branched polymer (Gum Arabic). These dispersions provided separation of the MWCNTs and their individual incorporation into the PEO nanofibers by subsequent electrospinning. The focus of this work is on the development of axial orientations in these multicomponent nanofibers. A theoretical model is presented for the behavior of rodlike particles representing CNTs in electrospinning. Initially the rods are randomly oriented, but due to the sinklike flow in a wedge they are gradually oriented mainly along the stream lines, so that straight CNTs are almost oriented upon entering the electrospun jet. The degrees of orientation of polymer, surfactant, and MWCNT were studied using X-ray diffraction and transmission electron microscopy. Oriented ropes of the nanofibers were fabricated in a converging electric field by a rotating disk with a tapered edge. A high degree of alignment of PEO crystals was found in electrospun nanofibers containing only PEO, as well as PEO/SDS. The latter also exhibited a high degree of alignment of the SDS layers. The axial orientation of PEO and SDS is significantly reduced in MWCNT-containing nanofibers. Transmission electron microscopy (TEM) images indicated that the MWCNTs were embedded in the nanofibers as individual elements, mostly aligned along the fiber axis. Nevertheless, there are also many cases in which the nanotubes appear twisted, bent, or with other irregularities. Comparison of cryo-TEM images of vitrified MWCNT dispersions with TEM images of the raw nanotubes indicated that sonication during the dispersion process may be responsible for the irregularities observed in some of the nanotubes.

## Introduction

Since the discovery of carbon nanotubes (CNTs) by Iijima,<sup>1</sup> they have been the focus of intense investigations due to their new and unique properties. These offer the potential for exciting applications such as ultrastrong wires, nanoelectronic devices, field electron emitters, nanopropes, nanocomposite materials, and more.<sup>2</sup> However, realization of their excellent properties in many cases is hampered by processing difficulties. As-produced CNTs, in particular single-walled nanotubes (SWCNTs), form tight long bundles due to van der Waals interaction. The bundles can form a dense entangled network. A significant challenge is to introduce the individual carbon nanotubes in an oriented assembly in order to express their unique anisotropic properties. Thus, separation of these bundles and dispersion and alignment of the individual nanotubes are crucial steps for several applications.

Several approaches are pursued in order to obtain stable dispersions of CNTs for processing. Aqueous dispersions are achieved with surfactants or amphiphilic polymers which can adsorb onto the hydrophobic nanotubes, such as sodium dodecyl sulfate (SDS),<sup>3</sup> poly(vinyl pyrrolidone) (PVP),<sup>4</sup> and the natural polysaccharide Gum Arabic.<sup>5</sup>

Processing CNT dispersions and alignment of the individual nanotubes or bundles is an important objective.

Several techniques have been applied to this end, such as deposition of carbon nanotubes suspension under magnetic field,<sup>6</sup> mechanical stretching of a polymer/nanotube composite film,<sup>7,8</sup> and synthesis of aligned nanotubes by deposition of nanotubes onto chemically modified substrate.<sup>9</sup> Recently, Vigolo and co workers<sup>3,10,11</sup> successfully developed a direct technique to spin carbon nanotubes from an aqueous dispersion in SDS. The dispersion is injected into a rotating solution of poly(vinyl alcohol) (PVA), whereby shear forces induce a measure of alignment. Replacement of the SDS adsorbed on the CNTs by PVA induces aggregation of the CNTs.

An interesting processing method that provides strong elongation of a polymer solution is electrospinning. The method produces polymer nanofibers of characteristic diameters ranging from a few to several hundred nanometers and is attracting much interest due to potential applications as high surface area membranes, electronic devices, biomedical applications, and nanocomposite

\* To whom correspondence should be addressed: e-mail, yachinc@tx.technion.ac.il.

<sup>†</sup> Department of Chemical Engineering.

<sup>‡</sup> Department of Mechanical Engineering.

(1) Iijima, S. *Nature* **1991**, *354*, 56–58.

(2) Ajayan, P. M.; Zhou, O. Z. *Top. Appl. Phys.* **2001**, *80*, 391–425.

(3) Vigolo, B.; Penicaud, A.; Coulon, C.; Sauder, C.; Paillet, R.; Journet, C.; Bernier, P.; Poulin, P. *Science* **2000**, *290*, 1331–1334.

(4) O'Connell, M. J.; Boul, P. J.; Ericson, L. M.; Huffman, C. B.; Wang, Y.; Haroz, E.; Kuper, C.; Tour, J.; Ausman, K. D.; Smalley, R. E. *Chem. Phys. Lett.* **2001**, *342*, 265–271.

(5) Bandyopadhyaya, R.; Nativ-Roth, E.; Regev, O.; Yerushalmi-Rozen, R. *Nano Lett.* **2001**, *1*, 1.

(6) Smith, B. W.; Benes, Z.; Luzzi, D. E.; Fischer, J. E.; Walters, D. A.; Casavant, M. J.; Schmidt, J.; Smalley, R. E. *Appl. Phys. Lett.* **2000**, *77*, 663–665.

(7) Bower, C.; Rosen, R.; Jin, L.; Han, J.; Zhou, O. *Appl. Phys. Lett.* **2002**, *74*, 3317–3319.

(8) Jin, L.; Bower, C.; Zhou, O. *Appl. Phys. Lett.* **1998**, *73*, 1197–1199.

(9) Schlittler, R. R.; Seo, L. W.; Gimzewski, J. K.; Durkan, C.; Saifullah, M. S. M.; Welland, M. E. *Science* **2001**, *292*, 1136–1139.

(10) Launois, P.; Marucci, A.; Vigolo, B.; Bernier, P.; Derre, A.; Poulin, P. *J. Nanosci. Nanotechnol.* **2001**, *1*, 125–128.

(11) Poulin, P.; Vigolo, B.; Launois, P. *Carbon* **2002**, *40*, 1741–1749.

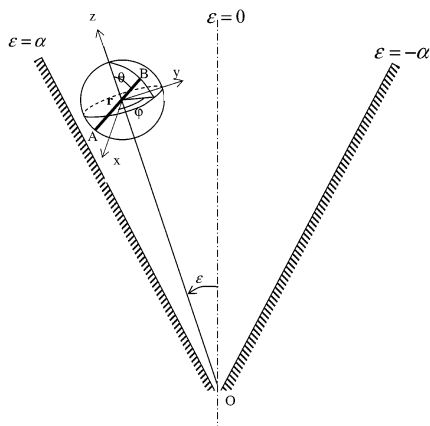


**Figure 1.** The wedge with a semiangle  $\alpha$ . Polar coordinates  $r$  (radial) and  $\epsilon$  (polar angle) are used to describe the position of a rod center. Spherical angular coordinates  $\theta$  and  $\varphi$  are used to characterize the orientation of the rodlike particle AB. Also the corresponding Cartesian coordinates  $x$ ,  $y$ , and  $z$  are shown.

materials. Its feasibility for incorporation of carbon nanotubes into nanofibers was demonstrated in recent works.<sup>12–14</sup> Nanofibers containing CNTs exhibit improvement in conductivity<sup>14</sup> and mechanical properties.<sup>12</sup> Still, the distribution and the alignment of the nanotubes in the nanofibers were rather random.

Here we use the electrospinning technique<sup>15</sup> to embed a small amount of carbon nanotubes in a polymer matrix, forming a composite nanofiber in which the individual CNTs can be discerned. The purpose of this work is to structurally characterize the composite nanofiber, with respect to the orientation of the polymer, surfactant, and carbon nanotubes within it. Furthermore, we present a model for the behavior of rodlike particles in a sink flow resembling electrospinning flow. In this work we utilize a novel approach for winding a continuous nanofiber on a rotating disk and assembly of well-aligned nanoropes.<sup>16</sup> Attention is given to preparation of stable nanotube dispersions, the quality of which may affect the distribution and alignment of CNTs during electrospinning.

### Theoretical Model

Consider a model which mimics behavior of rodlike particles representing CNTs in electrospinning. The jet originates from the tip of a conelike solution droplet similar to the Taylor cone.<sup>17</sup> Initially the rods are randomly oriented, but due to the sinklike flow in the cone they are gradually oriented mainly along the stream lines. That is the reason that straight CNTs are sucked into the electrospun jet as they are highly oriented along the spinning direction.

As a simplified model of such a situation, consider a planar sink flow in a wedge, known as the Hamel flow.<sup>18</sup> The flow is depicted in Figure 1. As a small rodlike particle

AB is sucked by the flow toward the sink at point O, its center moves along the corresponding stream line  $\epsilon = \text{constant}$ , whereas the particle is rotated by the flow. The particles are small; their length is on the order of  $10^{-5}$  cm. That is the reason that the Reynolds number of the particles is assumed to be small and the center translational velocity coincides with the local fluid velocity. On the other hand, at such a size the particles are already too big, which allows one to neglect rotational Brownian motion. That is the reason that only the flow-driven orientation is included in the Fokker–Planck equation describing particle orientation.

The only nonzero flow velocity component is the radial one,  $v = v_r$ . For the Hamel flow it is given by<sup>18</sup>

$$v = \frac{\nu}{r} F(\epsilon) \quad (1)$$

where  $\nu$  is the kinematic viscosity of the fluid and the function  $F(\epsilon)$  is found as a solution of the Navier–Stokes equations in the following approximate form

$$F = b \left\{ 3 \tanh^2 \left[ \left( -\frac{1}{2} b \right)^{1/2} (\alpha - \epsilon) + \beta \right] - 2 \right\} \quad (2)$$

where  $b < 0$  and  $\beta = \tanh^{-1}(2/3)^{1/2} = 1.146$ . The parameter  $(-b)$  plays the role of the Reynolds number related to the sink strength, and eq 2 is approximately valid for  $|b| \geq 50$ .

The Fokker–Planck equation describing the probability density function of particle orientation  $W(\varphi, \theta)$  in the Hamel flow reads

$$\begin{aligned} \frac{r^2}{\nu} \frac{\partial W \sin \theta}{\partial t} = & - \frac{\partial}{\partial \varphi} [\sin \theta \sin \varphi \cos \varphi F W] \\ & - \frac{\partial}{\partial \theta} \left[ \sin \theta \left( \sin \theta \cos \theta F + \sin^2 \theta \sin \varphi \frac{dF}{d\epsilon} + \right. \right. \\ & \left. \left. \sin \theta \cos \theta \sin^2 \varphi F \right) W \right] \quad (3) \end{aligned}$$

where the current position of the particle center  $r$  is given by

$$\frac{r^2}{2\nu} = F(\epsilon)t + \frac{r_0^2}{2\nu} \quad (4)$$

valid along a given stream line  $\epsilon = \text{constant}$ , and  $r_0$  is the initial particle location at  $t = 0$ .

At the initial condition for eq 3, the particles are randomly oriented

$$t = 0, \quad W = 1/4\pi \quad (5)$$

and the boundary conditions read

$$W(\theta) = W(\pi - \theta) \quad (6a)$$

$$W(\varphi) = W(\pi - \varphi) = W(\pi + \varphi) = W(2\pi - \varphi) \quad (6b)$$

which also means that the integral condition

$$\int_0^\pi \int_0^{2\pi} \sin \theta W d\varphi d\theta = 1 \quad (7)$$

holds.

In the present case we are interested only in the particles aligned in the flow plane  $\varphi = \pi/2$ . Denoting  $W(\theta, \pi/2) = \tilde{W}(\theta)$ , we obtain the equation describing their probability density function from eqs 3 and 4 as

(12) Ko, F.; Khan, S.; Ali, A.; Gogotsi, Y.; Naguib, N.; Yang, G.; Li, C.; Shimoda, H.; Zhou, O.; Bronikowski, M. J.; Smalley, R. E. *AIAA* **2002**.

(13) Ko, F.; Han, W. B.; Khan, S.; Rahaman, A.; Zhou, O. *ASC 16th Annu. Tech. Conf.* **2002**.

(14) Schreuder-Gibson, H.; Senecal, K.; Sennett, M.; Huang, Z.; Wen, J. G.; Li, W.; Wang, D.; Yang, S.; Tu, Y.; Ren, Z.; Sung, C. *Proc. Electrochem. Soc.* **2000**, 2000–2012.

(15) Reneker, D. H.; Yarin, A. L.; Fong, H.; Koombhongse, S. *J. Appl. Phys.* **2000**, *87*, 4531–4547.

(16) Theron, A.; Zussman, E.; Yarin, A. L. *Nanotechnology* **2001**, *12*, 384–390.

(17) Yarin, A. L.; Koombhongse, S.; Reneker, D. H. *J. Appl. Phys.* **2001**, *90*, 4836–4846.

(18) Rosenhead, L. *Laminar Boundary Layers*; Clarendon Press: Oxford, 1963; pp 144–150.

$$\left(2t + \frac{r_0^2}{\nu F}\right) \frac{\partial \tilde{W}}{\partial t} + \left(\sin 2\theta + \sin^2 \theta \frac{dF/d\epsilon}{F}\right) \frac{\partial \tilde{W}}{\partial \theta} = \tilde{W} \left(3 \sin^2 \theta - 3 \cos^2 \theta - 3 \sin \theta \cos \theta \frac{dF/d\epsilon}{F}\right) \quad (8)$$

Its solution satisfying the initial and boundary conditions is

$$\tilde{W}(\bar{t}, \theta) = \frac{1}{4\pi} \frac{1}{\left| \sin \theta \left( \cos \theta + \frac{dF/d\epsilon}{2F} \sin \theta \right) \right|^{3/2} \left| \frac{A}{1 + A^2} \left( 1 + \frac{dF/d\epsilon}{2F} A \right) \right|^{3/2}} \quad (9)$$

where  $\bar{t}$  is time  $t$  rendered dimensionless by  $r_0^2/\nu$ , and

$$A = \frac{1/(2F)}{[\bar{t} + 1/(2F)][\cos \theta + dF/d\epsilon \sin \theta/(2F)]/\sin \theta - (dF/d\epsilon)/(4F^2)} \quad (10)$$

In the particular case of the central stream line, where  $\epsilon = 0$ ,  $F(0) < F_0 < 0$ , and  $dF/d\epsilon = 0$ , eqs 9 and 10 yield

$$\tilde{W}(\bar{t}, 0) = \tilde{W}(\bar{t}, \pi) = \frac{1}{4\pi} \frac{1}{|2F_0 \bar{t} + 1|^{3/2}} \quad (11)$$

which shows that as  $\bar{t} \rightarrow -1/(2F_0)$  the values  $\tilde{W}|_{\theta=0}$  and  $\tilde{W}|_{\theta=\pi}$  tend to infinity and particles become fully aligned with the stream line. On the other hand, at the wedge boundary,  $\epsilon = \alpha$ , where  $F(\alpha) = 0$ , eqs 9 and 10 yield

$$\tilde{W} = \frac{1}{4\pi} \frac{1}{|\sin^2 \theta|^{3/2}} \frac{A^2}{|1 + A^2|} \quad (12)$$

where

$$A = \frac{1}{\bar{t}(dF/d\epsilon)|_{\epsilon=\alpha} + \cos \theta/\sin \theta} \quad (13)$$

It is seen that for  $\theta = 0$  or  $\pi$ ,  $A = tg\theta$ , whereas

$$\tilde{W} = 1/4\pi \quad (14)$$

which means that at the wall no flow-induced orientation takes place.

The general results given by eqs 9 and 10 are illustrated in Figure 2 for the stream line  $\epsilon = \alpha/10$ , the semiangle  $\alpha = \pi/6$  and the Reynolds number  $(-b) = 50$ . Alignment of the particles along the stream line manifested by a significant growth of  $\tilde{W}|_{\theta=0}$  and  $\tilde{W}|_{\theta=\pi}$  in time is clearly visible.

## Experimental Section

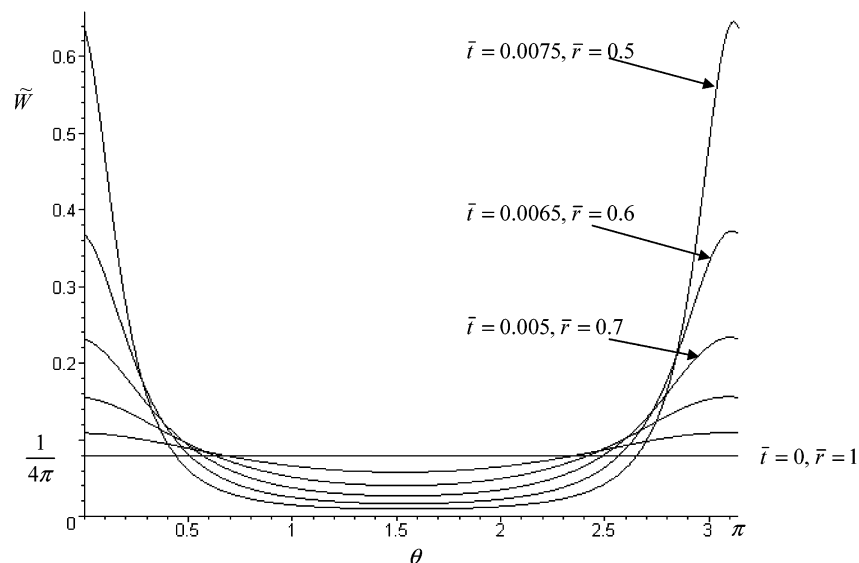
**Carbon Nanotubes and Dispersions.** Multiwalled CNTs (MWCNT) purchased from NanoLab were used for preparation of the dispersions. MWCNTs were dispersed in water in two ways using as the dispersing agent either SDS or Gum Arabic according to Table 1. Both dispersions were sonicated for 1 h in a 43 kHz Delta D2000 sonicator. The resulting dispersions were homogeneous and stable having a dark inklike appearance.

**Solutions for Electrospinning.** Solutions of poly(ethylene oxide) (PEO) in ethanol/water mixture were added to the MWCNTs/surfactant dispersions in order to achieve viscoelastic spinnable solutions. The PEO served also as the polymeric matrix of the electrospun nanofibers in which the nanotubes are embedded after solvent evaporation. The compositions of the dispersions and processing solutions are summarized in Table 1.

For comparison, nanofibers were also processed by electrospinning solutions of PEO (3% w/w in 40:60% v/v ethanol/water) and PEO/SDS (3% PEO and 1% SDS w/w in 40:60% v/v ethanol/water) without CNTs.

**Electrospinning.** The electrospinning technique is based on electrostatic forces drawing a jet of the polymer solution, which experiences high extension due to an electrostatically driven bending instability forming thin nanofibers.<sup>15</sup> Oriented ropes of the nanofibers were obtained in a converging electric field on a rotating disk with a tapered edge.<sup>16</sup> Electrospinning was carried out using air pressure of 0.1–0.3 kg/cm<sup>2</sup> to force the solution out of a syringe 0.5 mm in diameter at a voltage difference of 15 kV with respect to the collector. For X-ray diffraction measurements, nanofibers were collected on a disk rotating at 500 rpm.

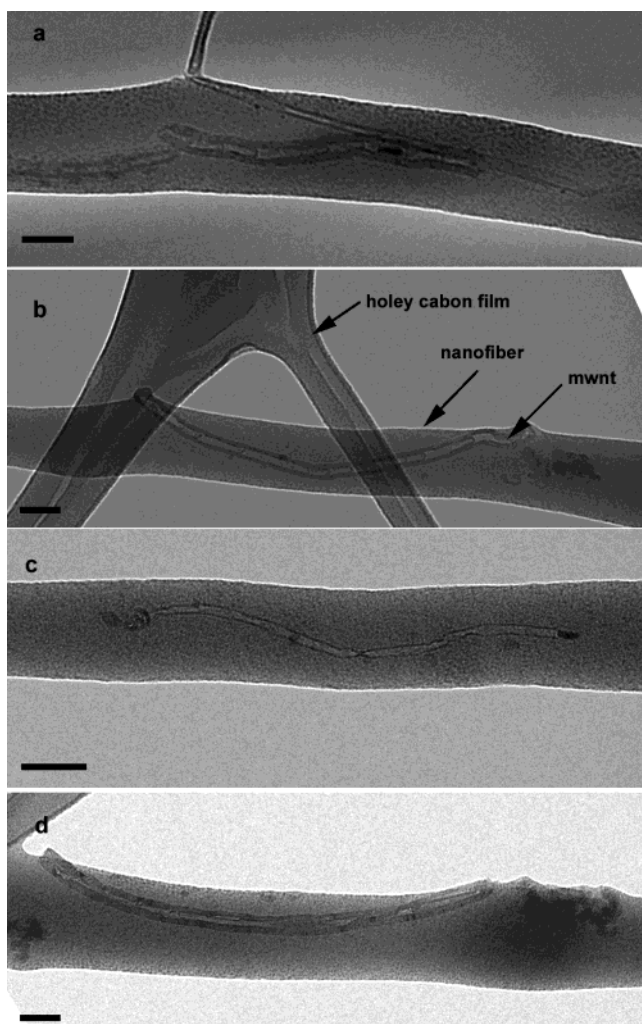
**Transmission Electron Microscopy.** The specimens for TEM analysis were prepared by direct deposition of the electrospun nanofibers onto a copper grid coated by a holey carbon film. The samples were investigated using low electron dose imaging and acceleration voltage of 120 kV in a Philips CM120 TEM. Images were recorded with a Gatan MultiScan 791 CCD camera, using the Gatan DigitalMicrograph 3.1 software package.



**Figure 2.** Probability density function for particles moving along the stream line  $\epsilon = \alpha/10$  in the case of the Reynolds number  $(-b) = 50$  and  $\alpha = \pi/6$ . The values of the dimensionless particle position  $\bar{r} = r/r_0$  are related via eq 4 to the dimensionless time  $\bar{t}$  by  $\bar{r} = (1 + 2F\bar{t})^{1/2}$ , where  $F(\alpha/10) = -29$ .

**Table 1. Parameters of Solutions Used in the Electrospinning Process**

	MWCNTs dispersion	PEO solution	electrospinning solution composition
1	0.35% (w/w) MWCNT 1% (w/w) SDS	6% (w/w) PEO ( $M_w = 600$ kDa) 40:60% (v/v) ethanol/water	50% (v/v) PEO solution 50% (v/v) MWCNT dispersion
2	0.35% (w/w) MWCNT 1% (w/w) Gum Arabic	4% (w/w) PEO ( $M_w = 900$ kDa) 40:60% (v/v) ethanol/water	74.5% (w/w) PEO solution 25.5% (w/w) MWCNT dispersion

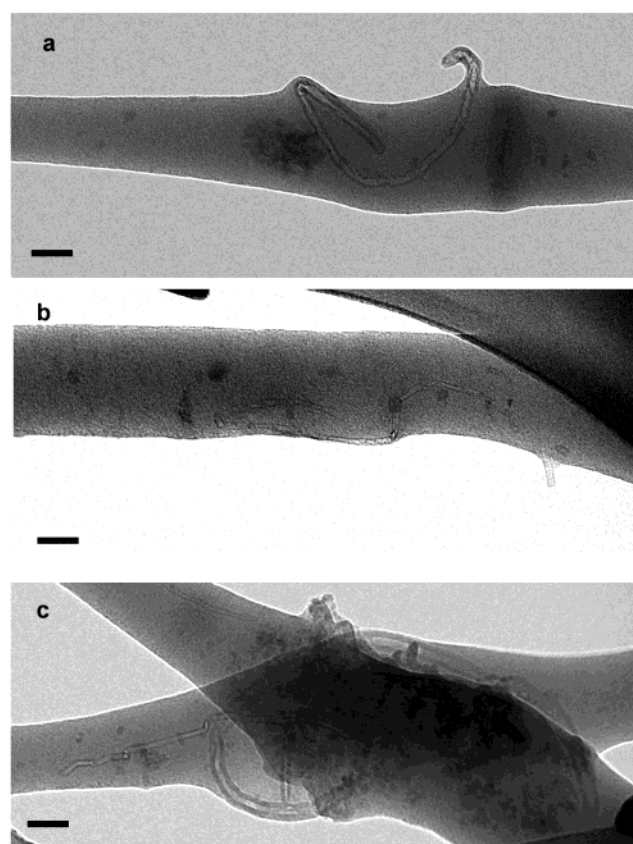
**Figure 3.** Oriented MWCNT in MWCNTs/PEO/SDS nanofibers. Bar = 50 nm.

Electron diffraction was recorded in selected area diffraction (SAD) mode using an aperture 280 nm in diameter and camera length of 970 mm.

**X-ray Diffraction.** X-ray diffraction patterns were recorded on flat film (Kodak MX125) in a "Warhus" vacuum camera with 0.025 in. pinholes (Blake), using Ni-filtered Cu  $K\alpha$  radiation from a sealed-tube generator (Philips PW1730). Both nanofiber axis and the photo film were perpendicular to the X-ray beam. The sample to detector distance was 5.31 cm for wide-angle diffraction and 19.5 cm for small-angle diffraction. Due to the small quantity of nanofibers in the rope, exposure times were about 15–20 h for wide-angle diffraction and 1–3 days for small-angle diffraction. To improve the measurement accuracy of the lattice and orientation parameters in small angle diffraction, additional measurements were performed using a small-angle diffractometer (Bruker Nanostar, KFF CU 2 K-90) with Cu  $K\alpha$  radiation, pinhole collimation that results in a beam 100  $\mu$ m in diameter, and a 10  $\times$  10 cm<sup>2</sup> two-dimensional position-sensitive wire detector that was positioned 65 cm behind the examined sample.

## Results and Discussion

The aqueous dispersions of MWCNT using either SDS or GA exhibited low shear and elongational viscosity so

**Figure 4.** Irregular arrangement of MWCNT in MWCNTs/PEO/SDS nanofibers. Bar = 50 nm.

that nanofibers could not be formed by electrospinning. Since solutions of PEO in ethanol/water mixtures provide adequate spinnability for electrospinning,<sup>15,16</sup> mixtures of aqueous MWCNT dispersion with PEO solutions were used in further experiments. Continuous nanofibers of controlled diameter were thus obtained either as an unoriented mat on a flat collector or as an oriented rope by deposition on a rotating wheel. Figures 3–6 show transmission electron microscopy (TEM) images of nanofibers containing MWCNTs/PEO/SDS and MWCNTs/PEO/GA. It is evident that individual MWCNTs were successfully embedded in the dispersing polymer/surfactant matrix. This indicates that the original dispersion contained individual nanotubes rather than aggregates or bundles.

In many regions of the electrospun nanofibers the embedded nanotubes appeared to be well-oriented along the fiber axis. Some examples of such nanofibers are shown in Figures 3 and 5 for nanotubes dispersed using SDS or GA, respectively. In these figures it can be seen that the nanotubes, while oriented along the fiber axis, nevertheless exhibit some degree of tortuosity. It is not clear whether this is due to their inherent structure that is characteristic of CNTs with topological defects<sup>19</sup> or to CNTs that are still not fully stretched by the electrospinning

(19) Rakov, E. G. *Usp. Khim.* **2000**, *69*, 41–59; *Russ. Chem. Rev.* **2000**, *69*, 35–52.

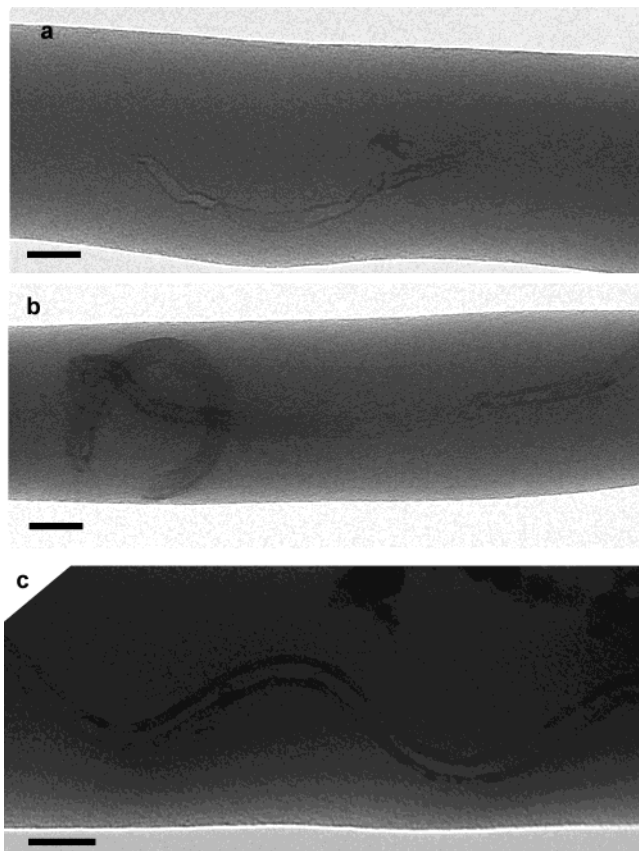
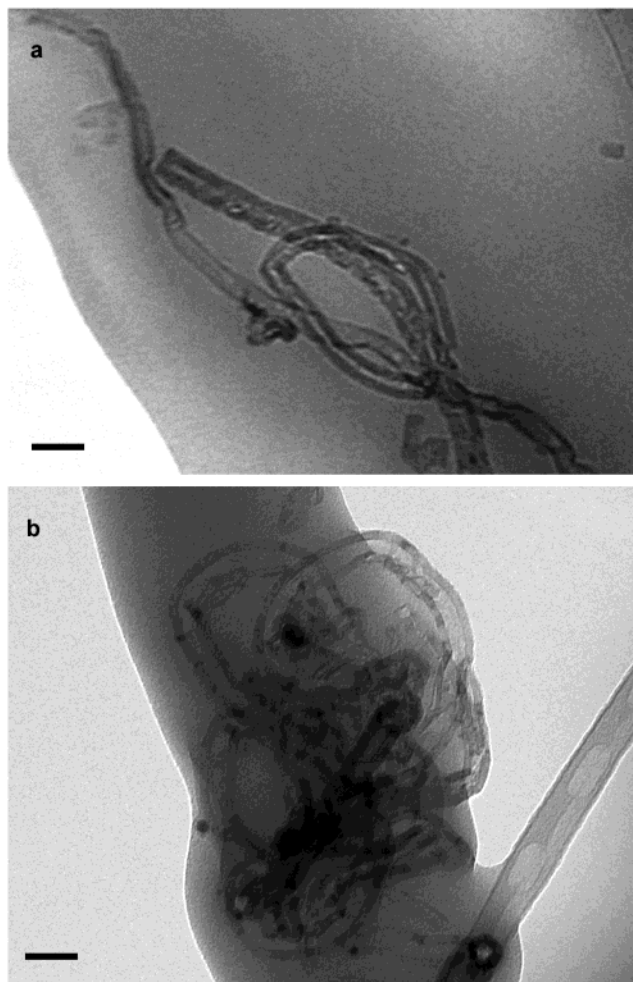


**Figure 5.** Oriented MWCNT in MWCNTs/PEO/GA nanofibers. Bar = 50 nm.

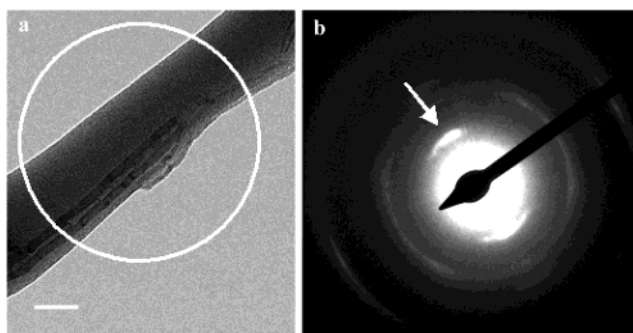
process. In some other regions (Figures 4 and 6) of the electrospun nanofibers the nanotubes appear in much more irregular conformations, exhibiting entanglements, knots, and even protrusions out of the nanofiber. It can be seen that these irregularities appear in conjunction with irregularities in the nanofiber diameter.

Figure 7 shows an oriented MWCNT embedded in a PEO/SDS nanofiber and the electron diffraction pattern from a region indicated as a circle in Figure 7a. The electron diffraction pattern (Figure 7b) is characteristic of multiwalled carbon nanotubes.<sup>1</sup> We were unable so far to observe electron diffraction from the PEO crystals within the nanofibers. This may be due to the sensitivity of the polymer crystallinity to electron radiation, compared to the carbon layers of the nanotubes.

The different appearances of the nanotubes in the nanofibers revealed the need to analyze the original dispersions. Cryo-TEM micrographs of PEO/GA/MWCNT dispersions are shown in Figures 8 and 9. It is clear that the dispersion consists of individual, well-separated nanotubes as was also indicated above by the images of electrospun nanofibers (Figures 3–6). However, both regular, smooth threadlike nanotubes (Figure 8) and looped, spiraled ones are observed (Figure 9). The shells of the irregular nanotubes seem to have suffered repeated pinches, which cause bending and twisting of the nanotubes, and in extreme cases may even cause highly deformed or spiral structures such as shown in Figure 9c. Some of the configurational defects could be found, for example, among the products of catalytic pyrolysis of hydrocarbons.<sup>19</sup> On the other hand, uniform shells are observed in the regular (extended) nanotubes as demonstrated in Figure 8. The uniform nanotubes are the ones that seem to be incorporated into the electrospun nanofiber in the oriented form while the bent and curled nanotubes



**Figure 6.** Irregular arrangement of MWCNT in MWCNTs/PEO/GA nanofibers. Bar = 50 nm.



**Figure 7.** Oriented MWCNT in MWCNTs/PEO/SDS nanofibers. (a) TEM image. Circle indicates the SAD aperture. Bar = 50 nm. (b) Electron diffraction pattern. Arrow indicates the carbon interlayer reflection at 3.48 Å.

cannot be fully aligned during the electrospinning process. Furthermore, a wide distribution in the nanotubes' diameter is observed (Figure 9a) which may lead to the variation of their position and orientation in the nanofiber. It seems that thick nanotubes, having many walls, are more sensitive to distortions during production and are thus incorporated into the nanofiber in an unoriented form. The more severe distortions may also be attributed to the sonication process during dispersion preparation. TEM images of raw MWCNTs, which have been suspended in methanol without sonication, are shown in Figure 10. It is clear that although the shells of the nanotubes are not

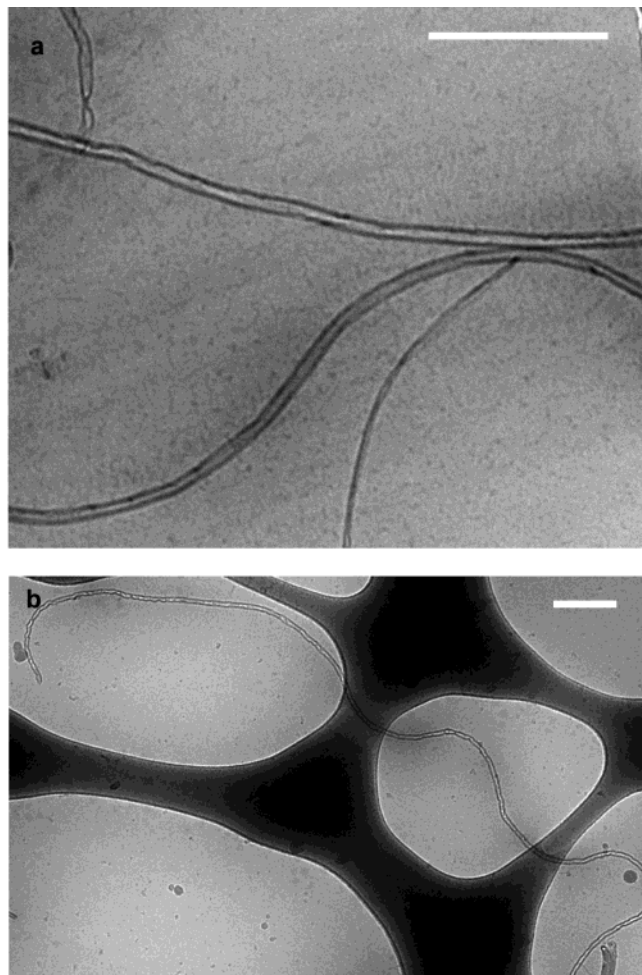


**Figure 8.** Cryo-TEM micrograph of MWNTs/GA dispersion. Bar = 200 nm.

perfect, severe irregularities, such as shown in Figure 9, are absent.

X-ray diffraction patterns from ropes of electrospun nanofibers are shown in Figure 11. When the electrospun solution contains only PEO (3%), the PEO fiber pattern is obtained (Figure 11a). The observed reflections fit the common monoclinic unit cell of PEO, in which the polymer conformation is a 7/2 helix.<sup>20</sup> The observed fiber pattern indicates that the PEO crystals are oriented with the chain axis preferentially aligned along the fiber axis. The degree of orientation can be evaluated from the azimuthal breadth of the first equatorial reflection (120) in the PEO fiber pattern, the full width at half-maximum (fwhm) of which is presented in Table 2. The diffraction from nanofibers containing PEO and SDS (Figure 11b) differs from that of PEO alone (Figure 11a) by exhibiting additional reflections due to the SDS crystals. The appearance of sharp equatorial reflections at small angles is due to the layered structure of SDS crystals, which are oriented with the layer normal perpendicular to the fiber axis. These reflections are shown more clearly in the small-angle scattering pattern in Figure 11, in which the camera length was changed from 5.31 to 19.5 cm. The layered structure of SDS in the nanofibers will be discussed further below. Weak off-meridional reflections, marked in Figure 11b, are also due to the SDS crystals. Figure 11c shows the diffraction pattern from the PEO/SDS/MWCNTs nanofiber rope. It is evident from the broad azimuthal arcs of the

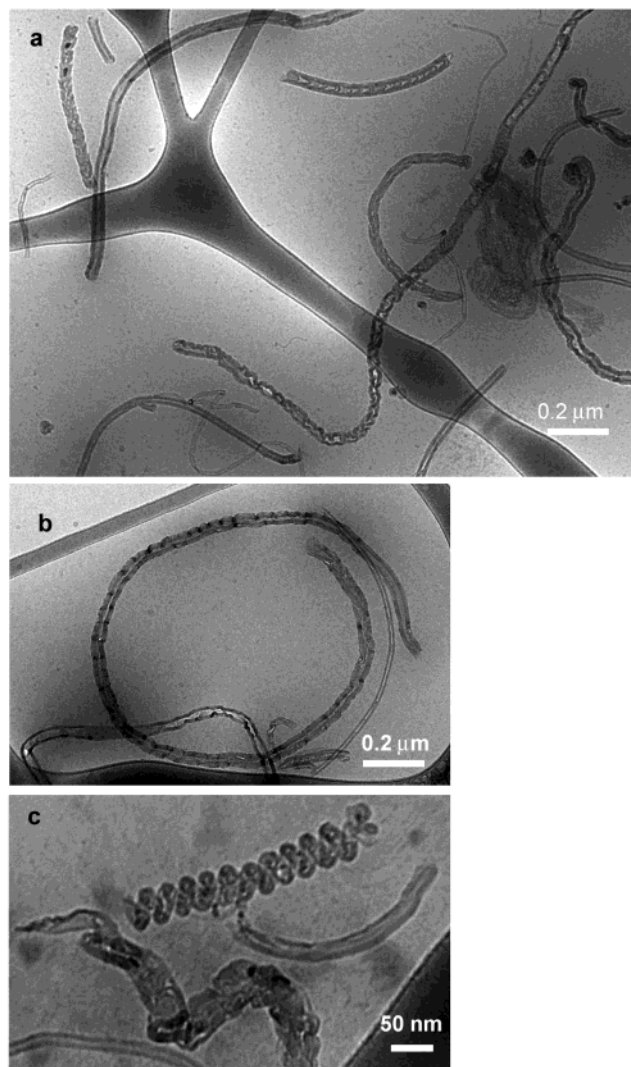


**Figure 9.** Cryo-TEM micrograph of irregular nanotubes in MWNTs/GA dispersion.

equatorial (120) reflections of the PEO crystals that they are now only poorly oriented along the fiber axis. The origin of the detrimental effect of the MWCNTs on the polymer orientation in the electrospun nanofibers is not clear. It may be related to the presence of the irregularly twisted and curled nanotubes in the spun dispersion, which hinders PEO orientation in their vicinity.

Figure 12 shows the small-angle scattering pattern from the PEO/SDS nanofiber rope, which exhibits several sharp equatorial reflections. A layered structure with alternating polar and apolar layers is common to all known SDS crystals.<sup>21</sup> The various SDS crystals differ, however, in the content of water molecules in the unit cell and the tilt angle of the alkyl chain relative to the layer normal.<sup>21</sup> The sharpness of the equatorial small-angle reflections indicates that the SDS layers are highly aligned with the layer normals perpendicular to the fiber axis. Their high degree of orientation, presented by the fwhm of the first two small-angle equatorial reflections (at about 40 and 24 Å), is also presented in Table 2. The Bragg spacings of the equatorial small-angle reflections do not fit a single layered lattice but rather a set of two coexisting ones, as shown in Table 3. The first set of reflections, listed in Table 3, corresponds to the monoclinic lattice described by Sun-

(20) Takahashi, Y.; Tadokoro, H. *Macromolecules* **1973**, *6*, 672–675.

(21) Smith, L. A.; Hammond, R. B.; Roberts, K. J.; Machin, D.; McLeod, G. *J. Mol. Struct.* **2000**, *554*, 173–182.

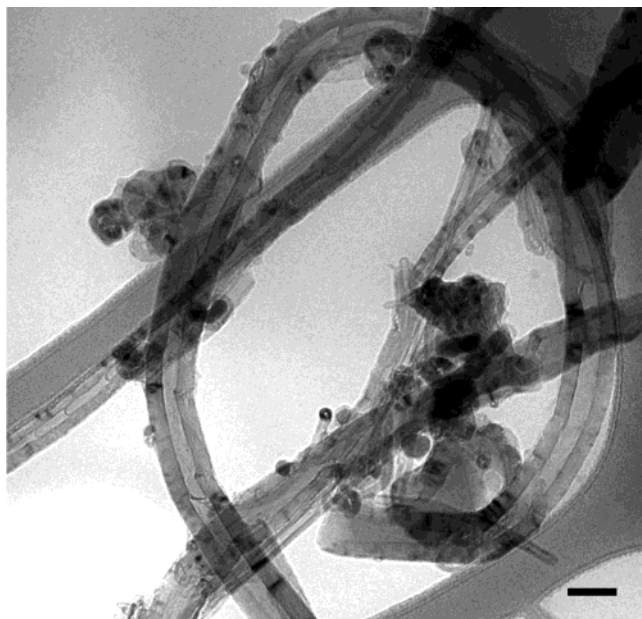


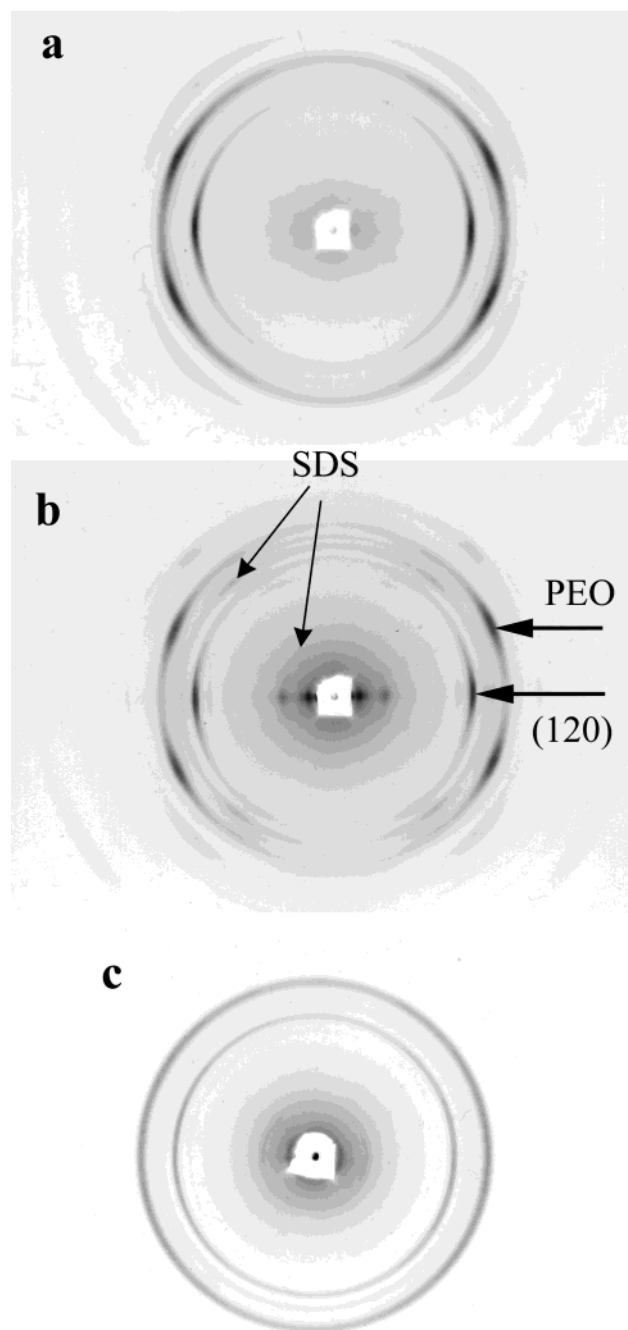
**Figure 10.** TEM micrograph of raw MWCNTs suspended in methanol without sonication. Bar = 50 nm.

**Table 2. Degree of Orientation of PEO and SDS Crystals in the Nanofibers, Given as the Azimuthal Breadth of the Equatorial Reflections (full width at half the peak maximum, fwhm)**

nanofiber composition	fwhm, deg		
	PEO (120)	SDS equatorial reflections (Table 3)	
		1st (40 Å)	2nd (24 Å)
PEO	13.5		
PEO/SDS	12.5	8.8	9.6
PEO/SDS/MWCNTs	83	35	32

dell,<sup>22</sup> with minimal water content (32:4 SDS/water molecules in the unit cell). In a control experiment, diffraction patterns were measured from SDS films cast from water and ethanol/water mixtures. Only reflections due to the Sundell monoclinic unit cell could be observed, as listed in Table 3. The second set of equatorial small-angle reflections do not seem to fit any of the known SDS unit cells. However the same reflections were observed in another control experiment, in which the diffraction pattern from films cast from SDS/PEO solutions were measured. The nature of this structure and its origin is currently under investigation. The results presented in Table 3 suggest that SDS molecules in nanofibers spun from solutions containing PEO exist as a mixture of two layered structures: a free SDS structure and the one due to interactions with the polymer.

A more detailed analysis of the small-angle reflections, obtained using a two-dimensional wire detector at a larger sample–detector distance (65 cm), is presented in Figure 13, which shows cross sections of scattering patterns along the meridian (fiber axis) and equatorial (normal to the fiber) directions. The intensity is plotted as a function of the scattering vector  $h (=4\pi \sin \theta/\lambda)$ , where  $\theta$  is half the scattering angle and  $\lambda$  is the wavelength). The equatorial scattering from the PEO/SDS nanofibers exhibits two prominent peaks, which are the first equatorial reflections (at Bragg spacings of 39.5 and 23.8 Å, respectively) of the two sets of SDS layers, as described above (Table 3).

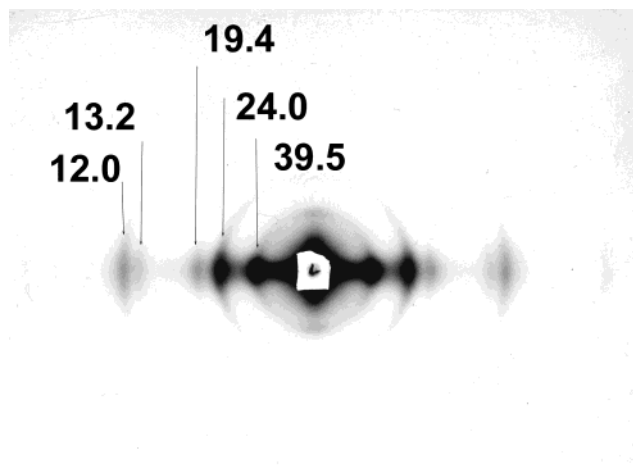


**Figure 11.** Wide-angle X-ray diffraction patterns of PEO-containing nanofiber ropes: (a) PEO; (b) PEO/SDS; (c) PEO/SDS/MWCNTs. The arrows in (b) mark off-meridional and equatorial reflections due to SDS. The small-angle reflections of SDS are shown in Figure 12. The fiber axis is vertical.

Appearance of weak reflections along the meridian at the 39.5 Å spacing indicates that some of the SDS crystals are aligned with their normal oriented along the fiber axis. At smaller angles, two weak reflections can be seen in the meridional scattering from PEO/SDS nanofibers (Bragg spacings about 157 and 81 Å), which may be identified as the first and second orders of the PEO long period. Since these reflections appear only along the meridian, this may indicate folding of the polymer chains into lamellae such that their normals are oriented along the fiber axis. Such a structure can occur in a “shish-kebab” morphology often observed in highly drawn fibers from polymer solutions or melt. Indirect evidence of a “shish-kebab” structure in

**Table 3. Bragg Spacings of SDS Layer Lattices in Nanofibers and Films**

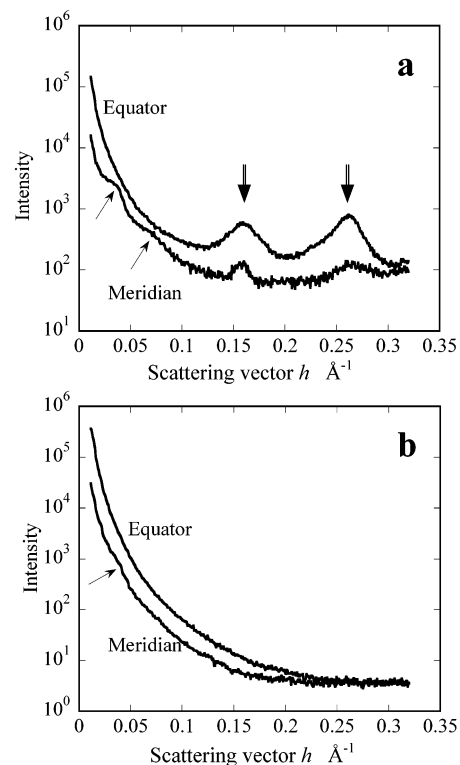
peak order	<i>hkl</i> monoclinic cell (Sundell) <sup>22</sup>	<i>d</i> spacing of SDS in PEO–SDS compositions, Å				
		monoclinic cell (Sundell) <sup>22</sup>	SDS film	PEO/SDS film	PEO/SDS nanofiber	PEO/SDS/MWCNTs nanofiber
1	2 0 0	38.9	39.5		39.5	39.1
2	4 0 0	19.5	19.4		19.4	
3	6 0 0	13.0	13.2		13.2	
5	10 0 0	7.8	8.0			
6	12 0 0	6.5	6.6	6.6	6.6	
7	14 0 0	5.56		5.9		
1				23.7	24.0	23.8
2				12.0	12.0	11.9
3				7.9	8.0	
4				6.0	6.0	

**Figure 12.** The small-angle X-ray diffraction pattern of PEO/SDS nanofiber rope. The fiber axis is vertical. The Bragg spacings (Å) of the main equatorial reflections are indicated on the picture.

electrospun PEO nanofibers was revealed in analysis of their tensile failure modes, which exhibited multiple necking which showed an inner fibrillar morphology.<sup>23</sup> It is interesting to point out that in the nanofibers containing only PEO, with about the same degree of orientation, only a very weak meridional reflection is observed, at about 77 Å (Figure 13b). The nature of PEO chain folding in PEO and PEO/SDS nanofibers and the particular role of SDS in this effect are not clear.

### Conclusions

The electrospinning process was used successfully to fabricate polymer nanofibers (PEO) in which multiwalled carbon nanotubes are embedded. Initial dispersion of MWCNTs in water was achieved using amphiphiles, either as small molecules (SDS) or as a high molecular weight, highly branched polymer (Gum Arabic). These dispersions provided separation of the MWCNTs and their individual incorporation into the PEO nanofibers by subsequent electrospinning. In this process a fluid jet originates from the tip of a conelike solution droplet similar to the Taylor cone. The focus of this work is on the development of axial orientations in these multicomponent nanofibers. A theoretical model is presented for the behavior of rodlike particles representing CNTs in electrospinning. Initially the rods are randomly oriented, but due to the sinklike flow in a wedge they are gradually oriented mainly along the stream lines, so that straight CNTs are sucked into the electrospun jet almost oriented. The degrees of

**Figure 13.** Cross sections of the small-angle X-ray pattern of PEO–SDS (a) and PEO (b) nanofibers in the equatorial and meridian directions. Single arrows point to weak meridional reflections assigned to chain-folded PEO lamellae, at Bragg spacings of (a) 157 and 81 Å and (b) 77 Å. Double arrows point to equatorial reflections assigned to SDS layers, at Bragg spacings of 39.5 and 24.0 Å.

orientation of polymer, surfactant, and MWCNTs were studied using X-ray diffraction and transmission electron microscopy. Oriented ropes of the nanofibers were fabricated in a converging electric field by a rotating disk with a tapered edge. The main conclusions of this study are as follows:

A high degree of alignment of PEO crystals, with the chain direction along the fiber axis, was found in electrospun nanofibers containing only PEO.

The high degree of polymer orientation was maintained in nanofibers containing PEO and SDS. Moreover, a high degree of alignment of the SDS layers was found in the spun nanofibers, so that the layer normals are predominantly perpendicular to the fiber axis.

The SDS molecules were found to exist in two forms of layered crystals. One is similar to known low-water-content crystals. The second is a new form that was also observed in films cast from SDS solutions containing PEO.

(23) Zussman, E.; Rittel, D.; Yarin, A. L. *Appl. Phys. Lett.* **2003**, *82*, 3958–3960.

TEM images indicated that the MWCNTs were embedded in the nanofibers as individual elements, mostly aligned along the fiber axis. Nevertheless, there are also many cases in which the nanotubes appear twisted, bent, or with other irregularities. The irregular nanotubes are poorly aligned.

Comparison of cryo-TEM images of vitrified MWCNT dispersions with TEM images of the raw nanotubes indicated that sonication during the dispersion process may be responsible for the irregularity observed in some of the nanotubes.

Current effort is directed at conditions which minimize

nanotube damage and at polymer nanofibers containing aligned single-walled nanotubes.

**Acknowledgment.** The work was partially supported by the Israel Science Foundation, the Israel Academy of Science, Grant N287/00-1, the U.S. Air Force–European Office of Aerospace Research and Development, Grant SPC-004066, and the Technion Fund for Promotion of Research: P. and E. Nathan Fund. TEM work was done at the Hannah and George Krumholz Advanced Microscopy Laboratory.

LA034234I